Desalination and Water Treatment
www.deswater.com
doi: 10.1080/19443994.2014.960467

56 (2015) 2127–2134
November

Taylor & Francis
Taylor & Francis Group

Removal of cobalt ions from aqueous solution by Ag/Fe bimetallic nanoparticles

Jiarui Huang[a,b], Fang Fang[b], Liyou Wang[b], Jae-Jin Shim[a,*]

[a]*School of Chemical Engineering, Yeungnam University, Gyeongsan 712749, Republic of Korea, Tel. +82 53 810 2587; Fax: +82 53 810 4631; email: jjshim@yu.ac.kr (J.-J. Shim)*
[b]*Center for Nano Science and Technology, College of Chemistry and Materials Science, Anhui Normal University, Wuhu 241000, P.R. China*

Received 2 April 2014; Accepted 21 August 2014

ABSTRACT

Ag/Fe bimetallic nanoparticles were synthesized by simple two-step method without nitrogen atmosphere. In the whole reaction process, polyvinyl pyrrolidone protected Fe nanoparticles and Ag/Fe bimetallic nanoparticles from oxidation. Moreover, the nanoparticles were characterized through high-resolution environment scanning electron microscope, transmission electron microscopy, X-ray diffraction, Fourier transform infrared spectroscopy, and energy dispersive spectrometer. The Fe nanoparticles and Ag/Fe bimetallic nanoparticles were used to remove Co(II) ions from aqueous solution. Experiments revealed that Ag/Fe bimetallic nanoparticles could quickly remove Co(II) ions from the aqueous solutions within 5 min, and the removal rate was up to 99%. Compared with Fe nanoparticles, as-prepared Ag/Fe bimetallic nanoparticles exhibit a higher adsorption capacity and faster reaction rate due to the numerous nanoscale Ag/Fe primary batteries, which indicates that the Ag/Fe bimetallic nanoparticles are highly promising for the applications of water treatment.

Keywords: Ag/Fe bimetallic nanoparticles; Nanoscale primary batteries; Remediation; Cobalt ion

1. Introduction

Heavy metals are important sources of environmental pollution, even in low concentration, since they are nondegradable and thus persistent. In the light of recent developments, in particular the mining industry and nonferrous metallurgy, that is accompanied by the growing pollution with heavy metal ions of wastewater [1]. Among the heavy metal pollutants, cobalt is one of the most widespread contaminants in the environment. Vast applications of cobalt in various arrays of products and processes such as alloys, batteries, catalysts, pigments, and coloring make this element as an important metal in various industries [2]. The presence of Co(II) metal ion in the environment is of important concern due to its toxicity and health effects on human, as well as radionuclide ^{60}Co(II) ions is considered to be one of the most dangerous radionuclides because of its long relatively half-life [3]. It can cause neuron toxicological disorders and genotoxicity in human beings, and in chronic cases may cause cancer [4,5]. High dose of cobalt may directly or indirectly cause detrimental health troubles such as paralysis, diarrhea, low blood pressure, lung irritation, and bone

*Corresponding author.

defects [6]. Hence, the removal of cobalt ions is very important from the health, economical, and environmental point of view.

A number of technologies have been developed over the years to remove toxic cobalt ions from water, including chemical precipitation [7], membrane separation [8], ion exchange [9], reverse osmosis [10], adsorption [11–13], and chemical reduction [14]. Among them, zero-valent iron (Fe^0) is usually used as chemical reductive agent to treat polluted groundwater and wastewater [15]. The high specific surface area and the high reactivity of Fe nanoparticles (NPs) make it a promising material for *in situ* remediation of groundwater contaminants, such as chromium ions, nitrobenzene, nitrate, arsenate and other chlorinated organic compounds, and heavy metal ions [16–20].

So far, at least two methods have been employed to achieve high reaction rates of zero-valent iron during its water treatment process. One is to construct a short-circuited battery-like cell with noble and active metal plates separated by an electrode gap. Another method is to form a hybrid powder through mechanically mixing the discrete noble metal particles and active metal powders, in which each hybrid particle forms a micro galvanic cell. While the micro battery-like cell has a principle disadvantage: the resistance in the electrical short circuit (external load) limits the reaction rate. In order to maximize the reaction rate, the electrode gap must approach zero. Yet, to sustain the reaction, reaction products must be flushed away from the reaction surfaces on time. This requires a small initial gap between the plates. In the powdered form, each grain of powder is a micro galvanic cell similar to the larger battery-like cell. A strong mechanical and electrical bond is necessary to provide a rapid reaction with a bimetallic galvanic cell. Besides, over the last decades the silver-based materials have been widely used as medicine and antimicrobial treatment material [21]. The addition of noble metal could make it better to make further progress on dealing with undrinkable water [22].

Here, Ag/Fe bimetallic nanoparticles were synthesized by simple two-step method. The adsorption property for Co(II) ions from aqueous solution of Ag/Fe bimetallic NPs was also discussed. The Ag/Fe bimetallic NPs consisting of Fe NPs and Ag NPs with diameters of approximately 70–100 nm and 3–10 nm, respectively, can be observed. Furthermore, Ag/Fe bimetallic NPs exhibit excellent adsorption property for Co(II) ions from aqueous solution. A comparative study of adsorption for Co(II) ions between as-prepared Ag/Fe bimetallic NPs and Fe NPs was performed to depict the superior adsorption properties of Ag/Fe bimetallic NPs.

2. Experimental

2.1. Synthesis

All chemical reagents were of analytic grade and used as received without further purification in this experiment. A simple two-step method was used to prepare Ag/Fe bimetallic NPs. Firstly, Fe NPs were synthesized with a simple approach without nitrogen atmosphere. In a typical experimental procedure, 0.417 g of ferric chloride hexahydrate ($FeCl_3{\cdot}6H_2O$) was dissolved in 150 mL of distilled water and 50 mL of ethanol mixed solution at room temperature. After that, 3.0 g of polyvinylpyrrolidone (PVP) and 0.59 g of sodium borohydride ($NaBH_4$) were added into the above solution under vigorous stirring. Then, the solution turned dark green and became black finally. After 30 min of stirring, the product was washed with distilled water and ethanol to clear away the redundant PVP and other ions. Fe NPs were selected by magnetic separation method during the washing process. The reductive reaction is as follows:

$$4Fe^{3+} + 3BH_4^- + 9H_2O \rightarrow 4Fe^0 \downarrow + 3H_2BO_3^- + 12H^+ + 6H_2 \uparrow \quad (1)$$

The bimetallic NPs were prepared through mixing the $AgNO_3$ aqueous solution with as-prepared Fe NPs under vigorous stirring at ambient temperature. Firstly, 0.15 g of Fe NPs was dispersed in 75 mL of ethanol. Then, 75 mL of 2 mM $AgNO_3$ aqueous solution was added into the above solution quickly under vigorous stirring at ambient temperature. After 15 min of redox reaction between the Ag^+ and Fe NPs, the products were washed with ethanol and acetone, and then stored in acetone. Similarly, Ag/Fe bimetallic NPs were selected by magnetic separation method during the washing process. The redox reaction describing the coating of Fe NPs with Ag NPs is as follows:

$$Fe^0 + 2Ag^+ \rightarrow Fe^{2+} + 2Ag \quad (2)$$

2.2. Analytical characterization

The products were characterized through environment scanning electron microscope (SEM, QUANTA 200FEG), transmission electron microscope (TEM, JEM-2100), X-ray diffraction (XRD, Shimadzu XRD-6000, with high-intensity Cu Kα radiation, with a wavelength of 1.54178 Å), Fourier transform infrared spectroscopy (FTIR, IRPrestige-21), and energy dispersive spectrometer (EDS, ESCALAB 250).

2.3. Adsorptive property measurements

All experiments were performed using a batch technique in Erlenmeyer flasks (25 mL capacity) under ambient conditions. The experiment was conducted by adding various amount of products to 10 mL of various concentrations of Co(II) solution. The Erlenmeyer flasks were shaken for a given time to achieve equilibrium. The concentrations of Co(II) ions were analyzed by an inductively coupled plasma mass spectrometry (ICP-MS). The amount of Co(II) ions adsorbed on NPs was calculated from the difference between the initial concentration and the equilibrium one. The sorption percentage and the distribution coefficient (K_d) are calculated from the following equations:

$$K_d = \frac{C_0 - C_e}{C_e} \times \frac{V}{m} \tag{3}$$

$$Q = (C_0 - C_e) \times \frac{V}{m} \tag{4}$$

$$W\% = \frac{C_0 - C_e}{C_0} \times 100\% \tag{5}$$

where C_0 is the initial concentration (mg L^{-1}), C_e is the equilibrium concentration (mg L^{-1}), m (g) is the mass of the adsorbent, and V (mL) is the volume of the suspension, $W\%$ is the adsorption efficient of the adsorbent. All experimental data were the average of duplicate or triplicate determinations. The relative errors of the data were under 5%.

3. Results and discussion

3.1. Morphology and microstructure

The SEM images of as-synthesized Ag/Fe bimetallic NPs were obtained with a high-resolution environment scanning electron microscope under high magnification. As shown in Fig. 1, the product is composed of large-scale, uniform spherical NPs with particle size of ca. 70–100 nm. The aggregation of Ag/Fe bimetallic NPs is attributed to the magnetic interactions between the adjacent metal NPs. TEM was employed to further characterize the sizes and distributions of the silver NPs and Fe NPs. Fig. 2(a) and (b) presents the TEM images of Fe NPs and Ag/Fe bimetallic NPs, respectively. Fig. 2(a) shows that the Fe NPs are covered with a PVP thin film. Here, the existence of PVP thin film protected the Fe NPs from oxidation. Fig. 2(b) shows a larger amount of small NPs (Ag) with diameters of ca. 3–10 nm emerging around the Fe NPs, and their distribution is uniform. To further verify the existence of PVP in the product, FTIR spectra of PVP and Fe/Ag bimetallic NPs were investigated as shown in Fig. 3. Comparing with the spectrum of PVP (Fig. 3(a)), the resonance peaks of C–H stretching (at 2,925 cm^{-1}), C=O stretching (at 1,658 cm^{-1}) were no change, the peak of CH_2 deformation (at 1,443 cm^{-1}) was strengthened and blue shift to 1,390 cm^{-1}. The peak of C–N stretching (at 1,287 cm^{-1}) was greatly weakened. The changes of the spectrum indicated that the PVP was strongly absorbed on the surface of Ag/Fe bimetallic NPs [23]. This result demonstrates that the PVP thin film coated on Ag/Fe bimetallic NPs has not been removed completely after washing with distilled water and ethanol several times, which is consistent with TEM results.

To better demonstrate the above hypothesis on Fe NPs and Ag NPs, XRD patterns of Fe NPs and Ag/Fe bimetallic NPs were investigated as shown in Fig. 4. XRD analysis verifies iron and silver existence, which supports the data extracted from TEM images. Fig. 4(a) shows a broad characteristic peak at 44.35°, indicating the existence of the (110) plane of cubic phase iron (JCPDS Card No. 85-1410). The low

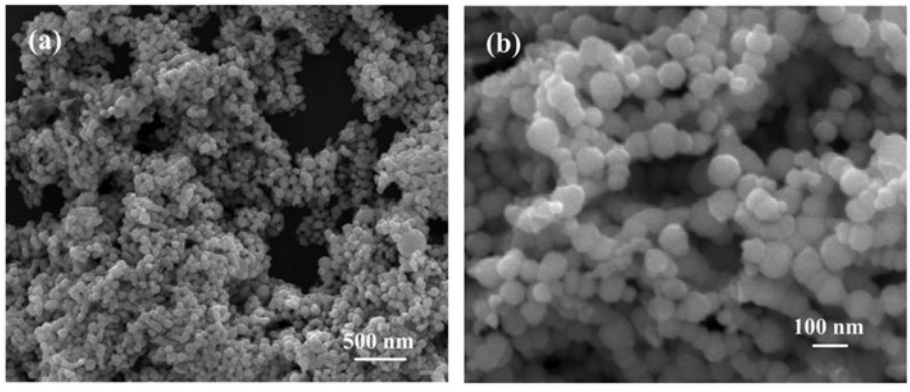

Fig. 1. SEM images of the Fe/Ag bimetallic NPs under (a) low magnification and (b) high magnification.

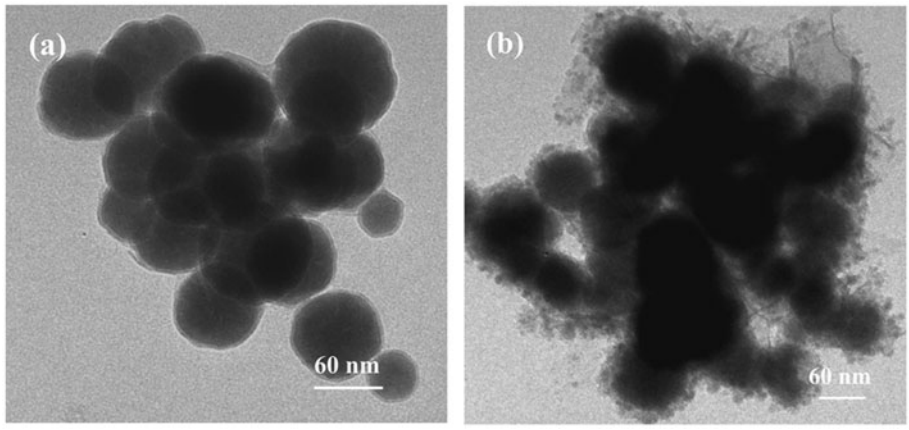

Fig. 2. TEM images of (a) Fe NPs and (b) Fe/Ag bimetallic NPs.

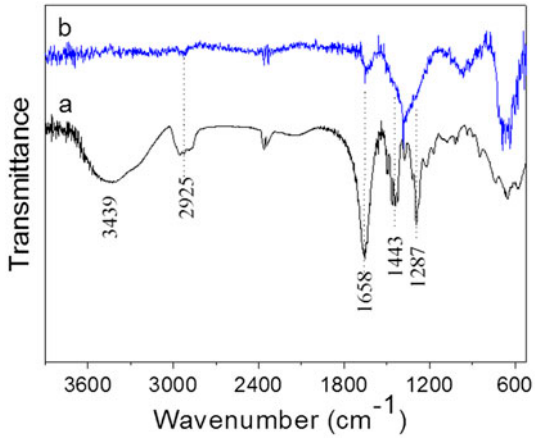

Fig. 3. FTIR spectra of (a) PVP and (b) Fe/Ag bimetallic NPs.

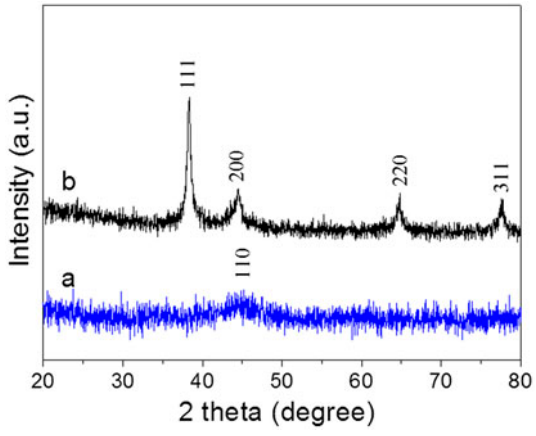

Fig. 4. XRD patterns of (a) Fe NPs and (b) Fe/Ag bimetallic NPs.

intensity of iron characteristic peak can be ascribed to poor crystallinity of the Fe NPs. In the case of Ag/Fe bimetallic NPs, the characteristic peaks at 38.26°, 44.47°, 64.71°, and 77.74° are indexed to the (111), (200), (220), and (311) planes of cubic phase silver (JCPDS Card No. 87-0719), respectively. No iron oxide phases are detected from the XRD patterns, indicating that Fe NPs and Ag/Fe bimetallic NPs were protected well by the PVP thin film from oxidation.

EDS study was done to further analyze the elemental composition of Ag/Fe bimetallic NPs (Fig. 5). Two clusters of characteristic peaks of iron and silver were identified, confirming the bimetallic structure of NPs. The main elements in the Ag/Fe bimetallic NPs product were Fe and Ag with a molar ratio of approximately 9:1. In addition, characteristic peaks of carbon, nitrogen, and oxygen were also identified, verifying the existence of PVP in the products.

3.2. Adsorptive property

Equilibrium adsorption is usually used to determine the capacity of the adsorbent. Several equilibrium adsorption models are available, and the most common ones are the monolayer adsorption developed by Langmuir (1918) and the multilayer adsorption by Freundlich (1906). The Langmuir adsorption model can be expressed as:

$$\frac{C_e}{Q_e} = \frac{C_e}{Q_L} + \frac{1}{Q_L K_L} \tag{6}$$

where C_e (mg L^{-1}) is the metal ion concentration in the solution at equilibrium, Q_e (mg g^{-1}) is the metal ion concentration on the sorbent at equilibrium, Q_L (mg g^{-1}) is the monolayer adsorption capacity of

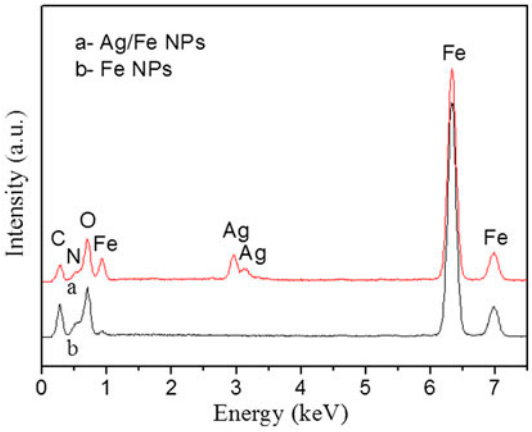

Fig. 5. EDS spectra of (a) Fe/Ag bimetallic NPs and (b) Fe NPs.

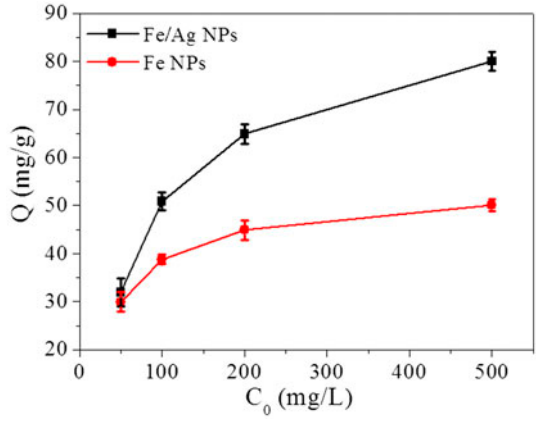

Fig. 6. Equilibrium adsorptions of Co(II) ions with Ag/Fe bimetallic NPs and Fe NPs (T = 25°C).

sorbent, and K_L (L mg^{-1}) is the Langmuir sorption constant, which represents enthalpy of sorption and should vary with temperature.

The Freundlich model can be expressed as:

$$\ln Q_e = \frac{1}{n}\ln C_e + \ln K_F \tag{7}$$

where K_F (mg^{1-n} L^n g^{-1}) and n are the Freundlich sorption constants, describing the sorbent capacity and the degree of nonlinearity between the solute concentration in the solution and the amount adsorbed at equilibrium [24]. The experimental data are simulated with the Langmuir and Freundlich models, respectively.

Fig. 6 shows equilibrium adsorptions of Co(II) ions with Ag/Fe bimetallic NPs and Fe NPs, respectively, in which different concentrations of Co(II) ions are adsorbed by Ag/Fe bimetallic NPs and Fe NPs. Fig. 7(a) and (b) show two kinds of equilibrium adsorption models. Table 1 was obtained via calculation with the formulas 6 and 7. From Table 1, the values of the coefficient of determination, R^2 of the Langmuir sorption isotherms are higher than 0.99, indicating a good fit of the monolayer Langmuir model to the adsorption of Co^{2+} on the Ag/Fe bimetallic NPs and Fe NPs. The Q_L value of Ag/Fe bimetallic NPs for Co^{2+} is 81.96 mg g^{-1}, which is much higher than that of Fe NPs, showing that the adsorption capacity of the Fe NPs is increased by modifying it with Ag NPs.

To obtain short-term time (0–1 h) dependences of Co(II) ions adsorption reaction with Ag/Fe bimetallic NPs and Fe NPs, 100 mg L^{-1} Co(II) ions reacted with 0.1 g L^{-1} Ag/Fe bimetallic NPs and 0.1 g L^{-1} Fe NPs, respectively, and the concentrations of Co^{2+} were analyzed via ICP-MS at 0, 1, 2, 5, 10, 15, 30, and 60 min. Fig. 8(a) and (b) indicate that the adsorption procedure of Co(II) ions with Ag/Fe bimetallic NPs is much faster than that of Fe NPs, completing within 5 min. The pseudo-second-order rate equation is used to simulate the kinetic adsorption, presented as following:

$$\frac{t}{Q_t} = \frac{1}{2K_2Q_e^2} + \frac{t}{Q_e} \tag{8}$$

where K_2 (g mg^{-1} h^{-1}) is the pseudo-second-order rate constant of adsorption, Q_t (mg g^{-1}) is the amount of Co(II) ions adsorbed on the surface of the NPs at time t (min), and Q_e (mg g^{-1}) is the equilibrium adsorption capacity. A linear plot feature of t/Q_t vs. t is achieved and inserted in Fig. 8. The K_2 value is calculated from the slope and the intercept is 0.04 g mg^{-1} h^{-1} of Ag/Fe bimetallic NPs, and the adsorption rate constant of Fe NPs is 0.0014 g mg^{-1} h^{-1}. The correlation coefficients ($R^2 > 0.999$) for the linear plots are very close to 1, indicating that kinetic adsorption is very well described by a pseudo-second-order rate equation.

To investigate the removal efficiency of Ag/Fe bimetallic, 0.1, 0.2, and 1.0 g L^{-1} Ag/Fe bimetallic NPs were used in the experiment as shown in Fig. 9. With the increase of amount of adsorbent, the removal efficiency increases accordingly. For 0.1 g L^{-1} Ag/Fe bimetallic NPs, the reduction efficiency is ca. 20% after 5 min. The reduction efficiencies increase to 70 and 99%, respectively, as the amounts of Ag/Fe bimetallic NPs increase to 0.2 and 1 g L^{-1}. It can be inferred that

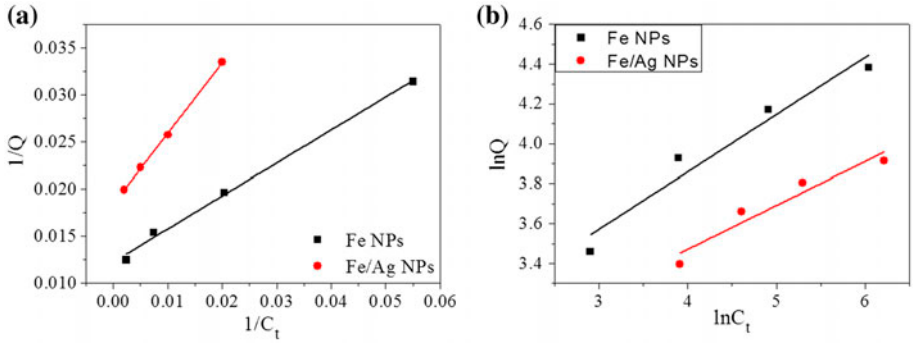

Fig. 7. Adsorption isotherms of Co(II) ions with Ag/Fe bimetallic NPs and Fe NPs: (a) Langmuir model and (b) Freundlich adsorption model.

Table 1
Parameters for Langmuir and Freundlich models of Co(II) ions adsorption on Fe NPs and Ag/Fe bimetallic NPs

	L-model			F-model		
	Q_L (mg g^{-1})	K_L	R^2	K_F	n	R^2
Fe NPs	54.259	0.024528	0.99927	13.3645	4.5469	0.89615
Ag/Fe bimetallic NPs	81.96	0.035	0.99442	15.076	3.48	0.92555

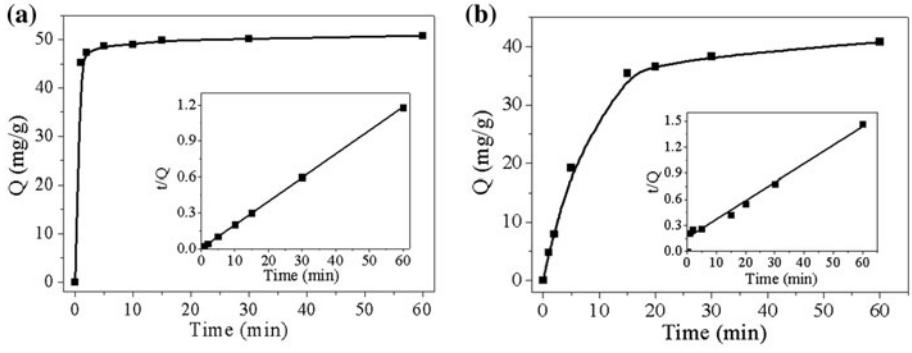

Fig. 8. Effect of setting time on the removal efficiency: (a) Ag/Fe bimetallic NPs and (b) Fe NPs (conditions: initial concentration, 100 mg L^{-1}; dose, 0.2 g L^{-1}). The insets are the linear plot features of t/Q_t vs. t.

undrinkable water contaminated by Co(II) ions can be quickly converted to drinkable water via adding the appropriate amount of Ag/Fe bimetallic NPs. Batch studies on the removal efficiency of Co(II) ions were carried out with different initial concentrations of Co(II) ions (5–500 mg L^{-1}). The removal efficiency was investigated by shaking the Co(II) ions solution with 1 g L^{-1} Ag/Fe bimetallic NPs. As shown in Fig. 10, the removal efficiencies were about 100% when the concentration of Co(II) ions was not more than 100 mg L^{-1}. After that, the removal efficiency decreased with the increase in the concentration of Co(II) ions. Therefore, the Ag/Fe bimetallic NPs with high removal efficiency and fast reaction rate are quite ideal material to deal with polluted water.

A conceptual model, as shown in Fig. 11, illustrates the reduction mechanism of Co(II) ions by Ag/Fe bimetallic NPs. Silver NPs coating on the surface of Fe NPs can improve the electrons transfer from core (Fe NPs) to the contaminant. Table 2 shows the electrode potentials. It can be seen that silver NPs and iron NPs can construct numerous nanoscale galvanic cells with high electrode potential. The nanoscale galvanic cells can improve the electrons transfer from Fe NPs to silver NPs and then the Co(II) ions are reduced by the electrons. In addition, the electrode potential of

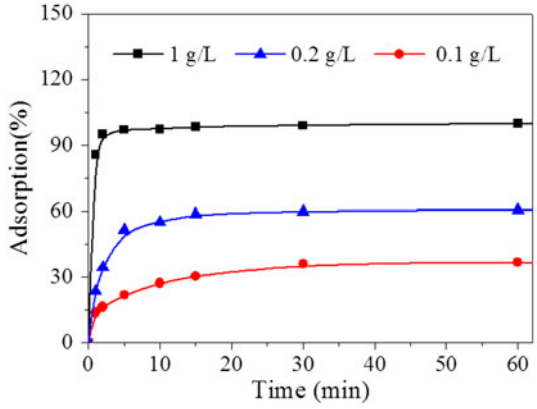

Fig. 9. Effect of dosage of Ag/Fe bimetallic NPs on the adsorption efficiency (conditions: adsorption time, 24 h; and initial concentration, 100 mg L^{-1}).

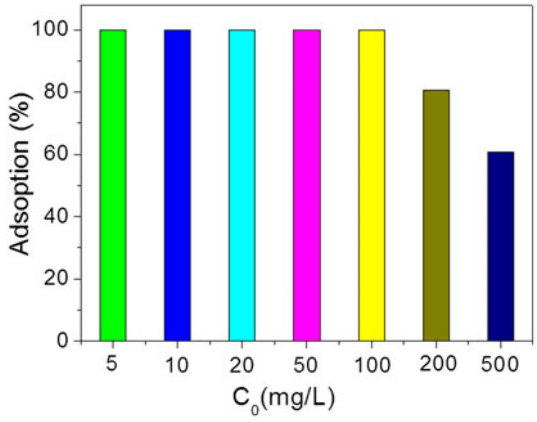

Fig. 10. Effect of the initial concentration of Co(II) ions on the adsorption efficiency (conditions: adsorption time, 24 h; and dose, 1 g L^{-1}).

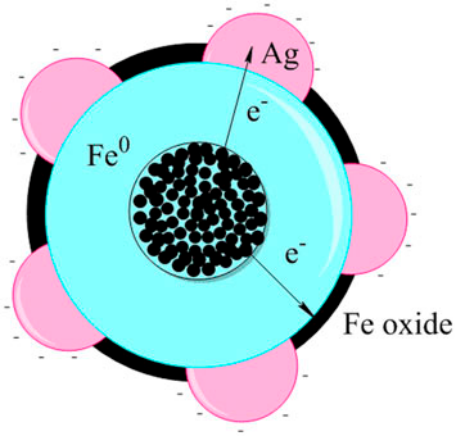

Fig. 11. The reduction mechanism of Co(II) ions by Ag/Fe bimetallic NPs.

Table 2
The electrode potentials

$\frac{1}{2}Fe + Ag^{+} = \frac{1}{2}Fe^{2+} + Ag$	$\Delta E^{\theta} = 1.023$ V
$Fe^{2+} + 2e^{-} = Fe$	$E^{\theta} = -0.447$ V
$Co^{2+} + 2e^{-} = Co$	$E^{\theta} = -0.28$ V

ferrous iron is higher than that of Co(II) ions. The ferrous iron product in the boundary layer can diffuse away from the surface of Ag/Fe bimetallic NPs and enter into the solution. While in the oxidative process of Fe NPs, iron oxide shell formed on the surface of Fe NPs is unsolvable in natural groundwater (pH ~8), which prevents the Fe NPs core from rapid oxidation and decreases the reduction rate of Co(II) ions in solution. Therefore, the Ag/Fe bimetallic NPs exhibit higher removal efficiency and faster reaction rate than those of Fe NPs.

4. Conclusions

In summary, Ag/Fe bimetallic NPs were synthesized by a facile simple two-step method without nitrogen atmosphere. The PVP thin film covered on the surface of Fe NPs protected them from oxidation in the whole process. The values of the coefficient (R^2) of the Langmuir sorption isotherms are higher than 0.99, indicating a good fit of the monolayer Langmuir model to the adsorption of Co^{2+} on Ag/Fe bimetallic NPs and Fe NPs. When compared with Fe NPs, Ag/Fe bimetallic NPs exhibit higher removal efficiency, higher adsorption capacity, and faster reaction rate. This is due to numerous nanoscale galvanic cells constructed by Ag NPs and Fe NPs, which can improve the electrons transfer from Fe NPs to silver NPs, and then the Co(II) ions are reduced by the electrons. Experiments revealed that the Ag/Fe bimetallic NPs could quickly remove Co(II) ions from the aqueous solutions within 5 min, and the removal efficiency was up to 99%. Therefore, Ag/Fe bimetallic NPs with high removal efficiency and fast reaction rate are quite ideal material to deal with undrinkable water contaminated by Co(II) ions in the case of emergency.

Acknowledgments

This work was supported by the National Nature Science Foundation of China (Project Nos. 21105001 and 21471005), NRF graphene project, National Key Research Institute Project, the Korea Basic Science Institute, and Priority Research Centers Program through the National Research Foundation of Korea (NRF) funded by the Ministry of Education (2014R1A6A1031189).

References

[1] X.L. Gao, C.T.A. Chen, Heavy metal pollution status in surface sediments of the coastal Bohai Bay, Water Res. 46 (2012) 1901–1911.

[2] K. Shang, Y.Z. Yang, J.X. Guo, W.J. Lu, F. Liu, W. Wang, Extraction of cobalt by the AOT microemulsion system, J. Radioanal. Nucl. Chem. 291 (2012) 629–633.

[3] S.W. Zhang, Z.Q. Guo, J.Z. Xu, H.H. Niu, Z.S. Chen, J.Z. Xu, Effect of environmental conditions on the sorption of radiocobalt from aqueous solution to treated eggshell as biosorbent, J. Radioanal. Nucl. Chem. 288 (2011) 121–130.

[4] Q. Wang, L. Chen, Y.B. Sun, Removal of radiocobalt from aqueous solution by oxidized MWCNT, J. Radioanal. Nucl. Chem. 291 (2012) 787–795.

[5] Y. Huang, L. Chen, H.L. Wang, Removal of Co(II) from aqueous solution by using hydroxyapatite, J. Radioanal. Nucl. Chem. 291 (2012) 777–785.

[6] R.W. Leggett, The biokinetics of inorganic cobalt in the human body, Sci. Total Environ. 389 (2008) 259–269.

[7] P. Ilaiyaraja, A.K. Singha Deb, D. Ponraju, B. Venkatraman, Removal of cobalt from aqueous solution using xanthate functionalized dendrimer, Desalin. Water Treat. 52 (2014) 438–445.

[8] J.H. Shao, S. Qin, W.X. Li, Y.L. He, Simultaneous recovery of nickel and cobalt from aqueous solutions using complexation–ultrafiltration process, Sep. Sci. Technol. 48 (2013) 2735–2740.

[9] Y. Aşçı, S. Kaya, Removal of cobalt ions from water by ion-exchange method, Desalin. Water Treat. 52 (2014) 267–273.

[10] M.G. Khedr, Nanofiltration and low energy reverse osmosis in rejection of radioactive isotopes and heavy metal cations from drinking water sources, Desalin. Water Treat. 2 (2009) 342–350.

[11] H.L. Wang, P. Zhang, X.K. Ma, S.W. Jiang, Y. Huang, L.F. Zhai, S.T. Jiang, Preparation, characterization of electrospun meso-hydroxylapatite nanofibers and their sorptions on Co(II), J. Hazard. Mater. 265 (2014) 158–165.

[12] F. Fang, L.T. Kong, J.R. Huang, S.B. Wu, K.S. Zhang, X.L. Wang, B. Sun, Z. Jin, J. Wang, X.J. Huang, J.H. Liu, Removal of cobalt ions from aqueous solution by an amination graphene oxide nanocomposite, J. Hazard. Mater. 270 (2014) 1–10.

[13] S. Rengaraj, S.H. Moon, Kinetics of adsorption of Co (II) removal from water and wastewater by ion exchange resins, Water Res. 36 (2002) 1783–1793.

[14] M.J. Wilkins, F.R. Livens, D.J. Vaughan, J.R. Lloyd, I. Beadle, J.S. Small, Fe(III) reduction in the subsurface at a low-level radioactive waste disposal site, Geomicrobiol. J. 27 (2010) 231–239.

[15] W.S. Orth, R.W. Gillham, Dechlorination of trichloroethene in aqueous solution using Fe^0, Environ. Sci. Technol. 30 (1995) 66–71.

[16] W.L. Yan, A.A. Herzing, C.J. Kiely, W.X. Zhang, Nanoscale zero-valent iron (nZVI): Aspects of the core-shell structure and reactions with inorganic species in water, J. Contam. Hydrol. 118 (2010) 96–104.

[17] X.Y. Li, M. Zhang, Y.B. Liu, X. Li, Y.H. Liu, R. Hua, C.T. He, Removal of U(VI) in aqueous solution by nanoscale zero-valent iron(nZVI), Water Qual. Expo. Health 5 (2013) 31–40.

[18] Y. Xu, W.X. Zhang, Subcolloidal Fe/Ag particles for reductive dehalogenation of chlorinated benzenes, Ind. Eng. Chem. Res. 39 (2000) 2238–2244.

[19] D.L. Wu, Y.H. Shen, A.Q. Ding, M.Y. Qiu, Q. Yang, S.S. Zheng, Phosphate removal from aqueous solutions by nanoscale zero-valent iron, Environ. Technol. 34 (2013) 2663–2669.

[20] D. Sparis, C. Mystrioti, A. Xenidis, N. Papassiopi, Reduction of nitrate by copper-coated ZVI nanoparticles, Desalin. Water Treat. 51 (2013) 2926–2933.

[21] R. Kumar, H. Münstedt, Silver ion release from antimicrobial polyamide/silver composites, Biomaterials 26 (2005) 2081–2088.

[22] O. Pana, C. Leostean, M.L. Soran, M. Stefan, S. Macavei, S. Gutoiu, V. Pop, O. Chauvet, Synthesis and characterization of Fe–Pt based multishell magnetic nanoparticles, J. Alloys Compd. 574 (2013) 477–485.

[23] H.S. Wang, X.L. Qiao, J.G. Chen, X.J. Wang, S.Y. Ding, Mechanisms of PVP in the preparation of silver nanoparticles, Mater. Chem. Phys. 94 (2005) 449–453.

[24] V.B.H. Dang, H.D. Doan, T. Dang-Vu, A. Lohi, Equilibrium and kinetics of biosorption of cadmium (II) and copper(II) ions by wheat straw, Bioresour. Technol. 100 (2009) 211–219.